Deriving physical and unique bimodal soil Kosugi hydraulic parameters from inverse modelling

J. Fernández-Gálvez, J.A.P. Pollacco, L. Lilburne, S. Mcneill, S. Carrick, Laurent Lassabatère, Rafaël Angulo-Jaramillo

Advances in Water Resources 153 (2021) 103933

Contents lists available at ScienceDirect

Advances in Water Resources

journal homepage: www.elsevier.com/locate/advwatres

Deriving physical and unique bimodal soil Kosugi hydraulic parameters from inverse modelling

J. Fernández-Gálvez[a,b,*], J.A.P. Pollacco[b], L. Lilburne[b], S. McNeill[b], S. Carrick[b], L. Lassabatere[c], R. Angulo-Jaramillo[c]

[a] Department of Regional Geographic Analysis and Physical Geography, University of Granada, Spain
[b] Manaaki Whenua – Landcare Research, Lincoln, New Zealand
[c] UMR5023 Ecologie des Hydrosystèmes Naturels et Anthropisés, CNRS, ENTPE, Université de Lyon 1, Bouguenais, France

ARTICLE INFO

Keywords:
Kosugi hydraulic model
Dual porosity
Hydraulic parameters
Inverse modelling
Non-uniqueness

ABSTRACT

Hydraulic parameters define the water retention, $\theta(\psi)$, and the unsaturated hydraulic conductivity, $K(\theta)$, functions. These functions are usually obtained by fitting experimental data using inverse modelling. The drawback of inverting the hydraulic parameters is that they suffer from non-uniqueness and the optimal hydraulic parameters may not be physical. To reduce the non-uniqueness, it is necessary to invert the hydraulic parameters simultaneously from observations of $\theta(\psi)$ and $K(\theta)$, and ensure the measurements cover the full range of θ from saturated to oven dry. The challenge of using bimodal $\theta(\psi)$ and $K(\theta)$ compared to unimodal functions is that it requires double the number of parameters, one set for the matrix and another set for the macropore domain. The objective of this paper is to address this shortcoming by deriving a procedure to reduce the number of parameters to be optimized to obtain a unique physical set of bimodal soil Kosugi hydraulic parameters from inverse modelling. To achieve this, we (1) derive residual volumetric soil water content from the Kosugi standard deviation parameter of the soil matrix, (2) derive macropore hydraulic parameters from the water pressure head threshold between macropore and matrix flow, and (3) dynamically constrain the Kosugi hydraulic parameters of the soil matrix. The procedure successfully reduces the number of optimized hydraulic parameters and dynamically constrains the hydraulic parameters without compromising the fit of the $\theta(\psi)$ and $K(\theta)$ functions, and the derived hydraulic parameters are more physical. The robustness of the methodology is demonstrated by deriving the hydraulic parameters exclusively from $\theta(\psi)$ and K_s data, enabling satisfactory prediction of $K(\theta)$ even when no additional $K(\theta)$ data are available.

1. Introduction

Running hydrological models that solve the Richards equation requires knowledge of physical soil hydraulic parameters. The soil hydraulic parameters define the water retention, $\theta(\psi)$, and the unsaturated hydraulic conductivity, $K(\theta)$, functions (e.g. Brooks and Corey, 1964; van Genuchten, 1980; Kosugi, 1994). The hydraulic parameters are usually obtained by fitting measured values of the $\theta(\psi)$ and $K(\psi)$ to the corresponding $\theta(\psi)$ and $K(\theta)$ functions. However, a serious drawback of deriving the hydraulic parameters by inverse modelling is that they suffer from equifinality or non-uniqueness (Ines and Droogers, 2002; Ines and Mohanty, 2008; Pollacco et al., 2008b; Sonkar et al., 2019). Beven (1993) defines equifinality as when more than one set of parameters give acceptable simulations relative to a given measure of goodness of fit between simulated and measured values. Pollacco et al. (2008b) found that to reduce the *range equifinality* and obtain a unique set of hydraulic parameters, it is necessary to invert the hydraulic parameters simultaneously from observations of both $\theta(\psi)$ and $K(\theta)$, and that the measurements must cover the full range of θ from fully saturated to oven dry. However, it is rarely the case that we have such rich data sets.

It has been shown that non-uniqueness or equifinality problems cause a number of challenges in hydrological modelling (Pollacco et al., 2008a, 2008b; Pollacco and Angulo-Jaramillo, 2009), as follows:

- ***Linked parameters*** of inverted hydraulic parameters (Pollacco et al., 2008b) are sets of parameters that have a mathematical relationship between them, such that these parameters produce similar objective function values close to those obtained with the optimal parameter set. Linked parameters cause challenges for the inverse modelling algorithm and the identification of parameters. To avoid such problems, the mathematical formulations should be properly set up with no inter-correlated parameters.

* Corresponding author.
E-mail address: jesusfg@ugr.es (J. Fernández-Gálvez).

https://doi.org/10.1016/j.advwatres.2021.103933
Received 22 January 2021; Received in revised form 7 April 2021; Accepted 24 April 2021
Available online 15 May 2021

- ***Non-uniqueness solution*** results in sets of optimal hydraulic parameters with some of them exhibiting non-physical hydraulic values, which detaches the physical relationship between $\theta(\psi)$ and $K(\theta)$ (Pollacco et al., 2013b, 2017). This is an important limitation for physically based models that can preclude convergence when solving the Richards equation.
- ***Optimal non-physical hydraulic parameters*** cannot be physically interpreted and therefore cannot be used to model hydrological processes; for example, to derive the impact of tillage practices on the value of the hydraulic parameters describing the pore size distribution (Drewry et al., 2019).

In order to address these three potential issues that may arise when the hydraulic parameters are inverted without access to the full range of $\theta(\psi)$ and $K(\theta)$, it is important to derive methods to reduce the probability of obtaining non-physical soil hydraulic properties by preventing non-physical combinations of hydraulic parameter sets.

Typically, most studies perform the fit of observations to unimodal hydraulic functions, while bimodal structured soils are more the rule than the exception (Jarvis, 2007; McLeod et al., 2008). These soils have both macropores and micropores, with two-stage drainage (e.g. Carrick et al., 2010). Fast flow (macropore flow) can occur when the water pressure head exceeds the threshold needed to activate the macropore network, adding to the matrix flow. Below this threshold, only the matrix participates in the flow. The combination of these two stages is known as bimodal hydraulic behaviour, or dual permeability, and was the subject of previous characterizations (Lassabatere et al., 2019, 2014). By nature, these soils have a bimodal pore size distribution, and although soil structure is one of the main reasons for this, bimodal behaviour could also happen for purely textural reasons (e.g. Durner, 1994). Therefore, soils with bimodal pore systems cannot be adequately described by unimodal hydraulic functions.

In addition to the need to account for dual permeability behaviour, a proper choice of $\theta(\psi)$ and $K(\theta)$ should be made to adequately describe each pore size domain (macro versus micro/matrix). The $\theta(\psi)$ and $K(\theta)$ are often expressed as closed-form unimodal functions (e.g. Brooks and Corey, 1964; Clapp and Hornberger, 1978; van Genuchten, 1980). This paper adopts the Kosugi (1994) $\theta(\psi)$ and $K(\theta)$ functions, because this model presents a physical basis for the description of pore size (log-normal distribution), and their related parameters are physically sound. Soils have a large variation in pore radius, which, according to Kosugi (1996), follows a log-normal probability density function. Pollacco et al. (2017) and Romano and Nasta (2016) found improvement by using bimodal log-normal expressions (dual porosity models) compared to using unimodal $\theta(\psi)$ and $K(\theta)$, especially for top soils, which are biologically more active.

Pollacco et al. (2013b) showed that the hydraulic parameters of the Kosugi model can be constrained by deriving an empirical relationship between them. Nevertheless, the drawback of the Pollacco et al. (2013b) method is that **(a)** the derived methodology is purely empirical and may not work universally, and **(b)** the method was developed for soils with unimodal pore distribution and should be adapted to multi-modal soils. The challenge of using bimodal or dual permeability functions is that they require double the number of parameters, with as many as eight hydraulic parameters to be optimized (Pollacco et al., 2017), which can exacerbate the problems of non-uniqueness. To enable the use of bimodal hydraulic functions, we present new methods to reduce the number of hydraulic parameters by using principles of soil physics, such that the optimal set of the optimal hydraulic parameters is within physical limits. We reduce the non-uniqueness of optimised Kosugi hydraulic parameters by deriving the relationship between the parameters from principles of soil physics, which we apply to the bimodal $\theta(\psi)$ and $K(\theta)$ functions.

This paper is organised as follows: Section 2 presents the bimodal soil Kosugi hydraulic functions and outlines the physical set of constraints proposed for the hydraulic parameters to reduce non-uniqueness; Section 3 presents the experimental data and the numerical algorithm used to derive the soil hydraulic parameters; Section 4 evaluates the performance of the different constraints when deriving $\theta(\psi)$ and $K(\theta)$ under a range of scenarios and shows that the proposed method can also be used to infer $K(\theta)$ when only $\theta(\psi)$ and K_s data are available; and Section 5 summarises the main conclusions.

2. Theory

2.1. Bimodal Kosugi hydraulic functions

In this study, for convenience the water pressure head values are taken to be positive (i.e., $\psi > 0$) for unsaturated soils. Defining ψ_{MacMat} [L] as the water pressure head threshold between macropore and matrix, then fast flow (macropore flow) can occur when $\psi \le \psi_{MacMat}$ (ψ is small enough to activate the macropores), and matrix flow (soil water moves in the micropores) is when $\psi > \psi_{MacMat}$. The bimodal Kosugi log-normal probability density function is described by Pollacco et al. (2017) as:

$$\begin{cases} \frac{\partial\theta(\psi)}{\partial\psi} = \frac{\partial\theta_{Mat}(\psi)}{\partial\psi} + \frac{\partial\theta_{Mac}(\psi)}{\partial\psi} \\ \frac{\partial\theta_{Mat}(\psi)}{\partial\psi} = \frac{\theta_{sMacMat}-\theta_r}{\sigma\psi\sqrt{2\pi}} e^{-\frac{[\ln\psi-\ln\psi_m]^2}{2\sigma^2}} \\ \frac{\partial\theta_{Mac}(\psi)}{\partial\psi} = \frac{\theta_s-\theta_{sMacMat}}{\sigma_{Mac}\psi\sqrt{2\pi}} e^{-\frac{[\ln\psi-\ln\psi_{mMac}]^2}{2\sigma_{Mac}}} \\ \theta_r < \theta_{sMat} \leqslant \theta_s \end{cases} \quad (1)$$

where θ [L^3 L^{-3}] represents the *volumetric soil water content* (splitted between the volumetric soil water content in the soil matrix domain, θ_{Mat} [L^3 L^{-3}], and the volumetric soil water content in the soil macropore domain, θ_{Mac} [L^3 L^{-3}]) and ψ [L] the *water pressure head*, with $\psi > 0$ for unsaturated soils; θ_s [L^3 L^{-3}] and θ_r [L^3 L^{-3}] are the *saturated* and *residual volumetric soil water content*, respectively; $\ln\psi_m$ [L] (indicating the argument of ln in units of length, i.e., ψ_m in [L]) and σ [-] denote the *mean* and *standard deviation* of $\ln\psi$ [L], respectively, in the soil matrix domain; $\ln\psi_{mMac}$ [L] and σ_{Mac} [-] denote the *mean* and *standard deviation* of $\ln\psi$, respectively, in the soil macropore domain; and $\theta_{sMacMat}$ [L^3 L^{-3}] is the *saturated volumetric soil water content* that differentiates inter-aggregate pores (structural macropores) and matrix domains (intra-aggregate micropores).

Integrating Eq. (1) from 0 to ψ yields the Kosugi bimodal $\theta(\psi)$:

$$\begin{cases} \theta(\psi) = \theta_{Mat}(\psi) + \theta_{Mac}(\psi) \\ \theta_{Mat}(\psi) = \frac{1}{2}(\theta_{sMacMat} - \theta_r)\,\mathrm{erfc}\left(\frac{\ln\psi-\ln\psi_m}{\sigma\sqrt{2}}\right) + \theta_r \\ \theta_{Mac}(\psi) = \frac{1}{2}(\theta_s - \theta_{sMacMat})\,\mathrm{erfc}\left(\frac{\ln\psi-\ln\psi_{mMac}}{\sigma_{Mac}\sqrt{2}}\right) \end{cases} \quad (2)$$

where erfc is the complementary error function.

The bimodal *unsaturated hydraulic conductivity* expressed as a function of the effective saturation, $K(S_e)$, can be written according to (Pollacco et al., 2017) as:

$$\begin{cases} S_e = \frac{\theta-\theta_r}{\theta_s-\theta_r} \\ K(S_e) = K_{Mat}(S_e) + K_{Mac}(S_e) \\ K_{Mat}(S_e) = K_s \frac{\theta_{sMacMat}-\theta_r}{\theta_s-\theta_r}\sqrt{S_e}\left[\frac{1}{2}\mathrm{erfc}\left(\mathrm{erfc}^{-1}(2S_e) + \frac{\sigma}{\sqrt{2}}\right)\right]^2 \\ K_{Mac}(S_e) = K_s \frac{\theta_s-\theta_{sMacMat}}{\theta_s-\theta_r}\sqrt{S_e}\left[\frac{1}{2}\mathrm{erfc}\left(\mathrm{erfc}^{-1}(2S_e) + \frac{\sigma_{Mac}}{\sqrt{2}}\right)\right]^2 \end{cases} \quad (3)$$

where K_s [$L\,T^{-1}$] is the *saturated hydraulic conductivity* and S_e [-] denotes the *effective saturation*, such that $0 \le S_e \le 1$. Note that the model can be considered as unimodal if the following condition is met:

$$\theta_s - \theta_{sMacMat} < 0.01 \quad (4)$$

2.2. Constraining the Kosugi hydraulic parameters

Fitting measured $\theta(\psi)$ and $K(\psi)$ data on Eqs. (3) and (4) requires optimizing eight soil hydraulic parameters (θ_s, θ_r, σ, ψ_m, K_s, $\theta_{sMacMat}$, σ_{Mac},

Table 1
Feasible dynamic range of the optimized bimodal Kosugi hydraulic parameters.

	θ_s [m^3 m^{-3}]	θ_r [m^3 m^{-3}]	ψ_m [mm]	σ [-]	K_s [cm h^{-1}]	$\theta_{sMacMat}$ [m^3 m^{-3}]	ψ_{mMac} [mm]	σ_{Mac} [-]
Min	Max(θ)	0.0	ψ_{MacMat}	0.75	5.53E-3	0.75 θ_s	1	0.2
Max	0.65	0.2	1E8	4.00	288	θ_s	ψ_{MacMat}	2.0

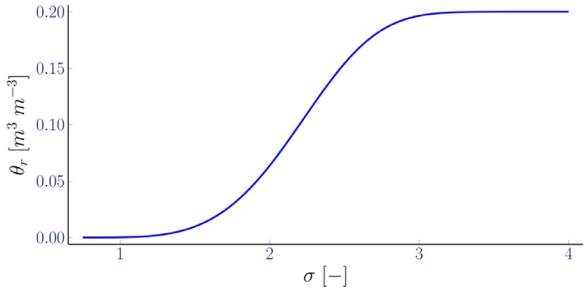

Fig. 1. Relationship between θ_r and σ described in Eq. (5), with $\theta_{rMax} = 0.2$, $\alpha_1 = 15$, and $\alpha_2 = 4$.

and ψ_{mMac}). The simultaneous estimation of all these parameters may cause problems of non-uniqueness. Non-unique hydraulic parameters were also obtained even when inverting only five hydraulic parameters using close-form unimodal hydraulic functions (Pollacco et al., 2013a, 2008b; Pollacco and Mohanty, 2012). Therefore, there is a need to reduce the number of parameters while providing hydraulic parameters that are physically sound.

2.2.1. Deriving θ_r from σ

The residual volumetric soil water content, θ_r, is a parameter without strict physical meaning, which is usually considered as the minimum amount of water left in the soil when the water pressure head is "infinite" (Du, 2020). θ_r is often set to zero, as it has been thought that this merely affects the goodness of fit for $\theta(\psi)$ and $K(\theta)$ (Clapp and Hornberger, 1978; Pollacco et al., 2013a, 2008b; Pollacco and Mohanty, 2012). Nevertheless, fixing θ_r at a constant value close to zero results in significant errors in the estimation of $\theta(\psi)$, especially for soils with significant clay fraction (e.g. Lee and Ro, 2014; Mohammadi and Meskini-Vishkaee, 2013). Pollacco et al. (2020) found that θ_r is related to the clay fraction and therefore could be correlated to σ. Large σ is associated with soils having high clay content. Therefore, a higher ψ is needed for water to be extracted from the smallest pores, resulting in higher θ_r, and vice versa for smaller σ. The following empirical expression is based on Pollacco et al. (2020), which relates θ_r to σ, is proposed:

$$\begin{cases} \sigma^* = \frac{\sigma - \sigma_{min}}{\sigma_{max} - \sigma_{min}} \\ \theta_r = \theta_{rMax} \frac{1 - e^{-\alpha_1 \cdot \sigma^*}}{1 - e^{-\alpha_1}} \end{cases} \quad (5)$$

where θ_{rMax} is set to 0.20 which was found by fitting $\theta(\psi)$ and $K(\theta)$ with laboratory data (e.g. Fernández-Gálvez et al., 2019; Pollacco et al., 2020, 2017, 2013b), the maximum value for θ_r that was found to be satisfactory, $\alpha_1 = 15$ and $\alpha_2 = 4$ are two optimized empirical parameters, σ^* [-] is the normalized σ, and σ_{min} [-] and σ_{max} [-] values are obtained from Table 1.

The relationship between θ_r and σ described in Eq. (5) is represented in Fig. 1, for σ values below 4 and the set of empirical parameters as indicated above. The shape of the curve shows the increase of θ_r with increasing σ, while the empirical parameters are responsible for the steepness of the slope before reaching θ_{rMax}. Using the relationship between θ_r and σ described in Eq. (5) and shown in Fig. 1 not only reduces the number of optimized parameters, but also reduces the non-uniqueness of σ by enforcing its physical meaning (Pollacco et al., 2020).

2.2.2. Deriving ψ_{mMac} and σ_{Mac} from ψ_{MacMat}

Structured soils have both matrix (inter-aggregate) pore spaces and macropore (intra-aggregate) pore spaces, where ψ_{MacMat} is the water pressure head boundary between macropore and matrix. Thus, when the pores are saturated ($\psi < \psi_{MacMat}$), the flow is considered macropore flow, and when the soil is desaturated ($\psi > \psi_{MacMat}$), the flow is considered matrix flow. Carrick et al. (2010) found that ψ_{MacMat} ranges from 50 to 150 mm, with an average of 100 mm also in agreement with other authors (e.g. Jarvis, 2007). We assume that ψ_{MacMat} is a constant parameter and so it is fixed at 100 mm. This threshold is also in line with previous studies and values suggested for the tension to be applied for the deactivation of the macropore network (e.g. Lassabatere et al., 2019, 2014; Luxmoore, 1981; Timlin et al., 1994). To reduce the number of optimized parameters, and due to the narrow range of water pressure head in the macropore domain, it is assumed (following Pollacco et al., 2017; Eq. 15) that:

$$\psi_{mMac} = e^{\frac{\ln \psi_{MacMat}}{2}} = \sqrt{\psi_{MacMat}} \quad (6)$$

Moreover, we assume that $\theta_{Mac}(\psi_{MacMat}) \approx 0$ in Eq. (2), and since $\theta(\psi)$ is a log-normal distribution we derive the following relationship computed with a typical value of $P_\sigma = 3$, establishing $\ln \psi_{MacMat}$ at a water pressure head higher than $\ln \psi_{mMac}$, which is three times the standard deviation of the logarithmic macropore size distribution.

$$\ln \psi_{MacMat} = \ln \psi_{mMac} + \sigma_{Mac} P_\sigma = \frac{\ln \psi_{MacMat}}{2} + \sigma_{Mac} P_\sigma \quad (7)$$

which results in:

$$\sigma_{Mac} = \frac{\ln \psi_{MacMat}}{2 P_\sigma} \quad (8)$$

Thus, by using Eqs. (6) and (8) with a fixed value of ψ_{MacMat}, it is possible to compute the Kosugi hydraulic parameters of the soil macropore domain without having to include them in the optimization scheme, which further reduces the number of parameters to optimize. The only macropore hydraulic parameter required is $\theta_{sMacMat}$.

2.2.3. Reducing non-uniqueness of the inverted σ and ψ_m

Pollacco et al. (2013b) showed that it is possible to reduce the non-uniqueness of the unimodal Kosugi hydraulic parameters by constraining the relationship between ψ_m and σ, taking advantage of the positive linear correlation between $\ln \psi_m$ and σ. Such correlation exists because the large median pore size (small ψ_m), which is characteristic of coarsely textured soils, is linked to a smaller dispersion in pore size (small σ). This relationship can be explained by the fact that when ψ_m is small, the soil tends to have single-grain texture (monodisperse) and so σ tends to be small. On the other hand, when ψ_m increases, corresponding to a smaller median pore size, which is characteristic of finer material, the soil becomes aggregated, where the soil is made up of a range of grain sizes (polydisperse), and so σ tends to be larger.

Pollacco et al. (2013b) found an empirical relation between these two parameters for a set of soils from the UNSODA (Leij et al., 1999) and HYPRES (Wösten et al., 1999) databases and used it to reduce the non-uniqueness of the inverted Kosugi hydraulic parameters. This relationship was also used by Fernández-Gálvez *et al.* (2019) to reduce the non-uniqueness of the hydraulic parameters derived from infiltration tests:

$$\sigma = P_{\sigma_1} \left(\ln \psi_m - 1 \right)^{P_{\sigma_2}} \quad (9)$$

where $P_{\sigma 1}$ and $P_{\sigma 2}$ are two fitting parameters [0-1].

Table 2
Nash–Sutcliffe efficiency coefficient (*NSE*) values and root mean squared errors (*RMSE*) from fitting bimodal Kosugi $\theta(\psi)$ and $K(\theta)$ with different constraints of the hydraulic parameters according to Section 2.2 and using the soil data described in Pollacco et al. (2020). θ_s is derived from total porosity, while σ, $\theta_{sMacMat}$ and K_s are optimized for all simulations. N_{opt} is the number of optimized parameters in each case.

Scenario	N_{opt}	θ_r	ψ_m	σ_{Mac}	ψ_{mMac}	$NSE_{\theta(\psi)}$	$NSLE_{K(\theta)}$	$\overline{NSE}$	$RMSE_{\theta(\psi)}$	$RMSLE_{K(\theta)}$	$\overline{RMSE}$
A	7	Opt	Opt	Opt	Opt	0.985	0.989	**0.987**	0.0078	0.0003	**0.0040**
B	6	$\theta_r(\sigma)$	Opt	Opt	Opt	0.973	0.987	**0.980**	0.0108	0.0004	**0.0056**
C	5	$\theta_r(\sigma)$	Opt	$\sigma_{Mac}(\psi_{MacMat})$	Opt	0.972	0.972	**0.972**	0.0111	0.0005	**0.0058**
D	5	$\theta_r(\sigma)$	Opt	Opt	$\psi_{mMac}(\psi_{MacMat})$	0.970	0.958	**0.964**	0.0112	0.0008	**0.0060**
E	4	$\theta_r(\sigma)$	Opt	$\sigma_{Mac}(\psi_{MacMat})$	$\psi_{mMac}(\psi_{MacMat})$	0.967	0.952	**0.960**	0.0117	0.0009	**0.0063**
F	5	Opt	Opt: $\psi_m(\sigma)$	$\sigma_{Mac}(\psi_{MacMat})$	$\psi_{mMac}(\psi_{MacMat})$	0.953	0.894	**0.924**	0.0133	0.0013	**0.0073**
G	4	$\theta_r(\sigma)$	Opt: $\psi_m(\sigma)$	$\sigma_{Mac}(\psi_{MacMat})$	$\psi_{mMac}(\psi_{MacMat})$	0.952	0.863	**0.908**	0.0138	0.0014	**0.0076**

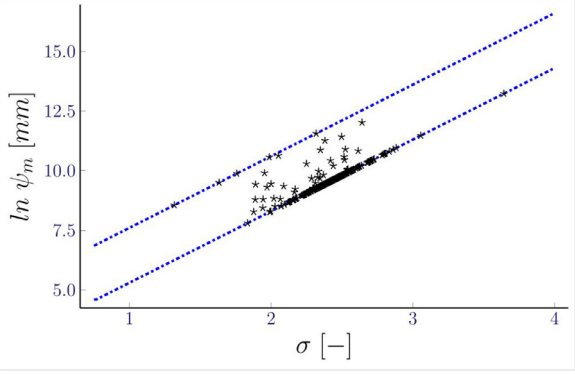

Fig. 2. Relationship between σ and ln ψ_m using Eq. (12) to reduce non-uniqueness of the hydraulic parameters for the set of studied soils. The two dashed lines represent the upper and lower limits of the dynamic constraint.

Nevertheless, the relationship shown in Eq. (9) is purely empirical and only applicable to the unimodal Kosugi hydraulic functions. Therefore, a physical relationship between ψ_m and σ for the bimodal Kosugi hydraulic functions is proposed, in which the feasible range of ψ_m is derived from σ.

Similarly to Eq. (7), the following expression is set for the matrix pore space domain with $P_\sigma = 3$:

$$\ln\psi_{mMac} \leqslant \ln\psi_m - \sigma P_\sigma \leqslant \ln\psi_{MacMat} \tag{10}$$

where isolating ψ_m, gives:

$$e^{\ln\psi_{mMac}+\sigma P_\sigma} \leqslant \psi_m \leqslant e^{\ln\psi_{MacMat}+\sigma P_\sigma} \tag{11}$$

and using Eq. (6) gives:

$$\sqrt{\psi_{MacMat}}e^{\sigma P_\sigma} \leqslant \psi_m \leqslant \psi_{MacMat}e^{\sigma P_\sigma} \tag{12}$$

For illustration purposes, Fig. 2 shows the relationship between σ and ln ψ_m using the dynamic physical range to reduce non-uniqueness of the hydraulic parameters (Eq. (12)) for the set of studied soils described in Section 3.1 and using the additional constraints corresponding to scenario G in Table 2.

Fig. 3 illustrates an example of the normalized constrained bimodal hydraulic functions, $S_e(\psi)$ and $K_{Se}(\psi)$, for three different values of σ (0.75, 2.38, and 4.00) and its corresponding feasible range of ψ_m derived from Eq. (12) with $S_e(\theta_{sMac}) = 0.85$. The feasible range of ψ_m determines the shape of the curves, with values between the solid and dotted lines corresponding to each of the σ considered. The plot of the $K_{Se}(\psi)$ curve for $\sigma = 4$ and $\psi_m = 15$ shows a small artefact next to ln (1+ψ) = 1 due to the transformation ln (1+ψ) in the x-axis.

The dynamic physical feasible range of the optimized bimodal Kosugi hydraulic parameters is indicated in Table 1. As indicated in Section 2.2.2, ψ_{MacMat} is considered constant with a value of 100 mm.

The proposed parsimonious bimodal Kosugi $\theta(\psi)$ and $K(\theta)$ model requires only four parameters (ψ_m, σ, K_s and $\theta_{sMacMat}$) to be optimized; with ψ_{MacMat} set as a constant, ψ_{mMac} and σ_{Mac} derived from ψ_{MacMat} using Eqs. (6) and (8), respectively, θ_r derived from σ through Eq. (5), and θ_s derived from total porosity. Moreover, the non-uniqueness between ψ_m and σ is also reduced by Eq. (12) using the assumption that $\theta(\psi)$ and $K(\theta)$ are log-normal distributed. Therefore, the number of hydraulic parameters to be optimized is reduced from eight to four using the principles of soil physics.

3. Material and methods

3.1. Experimental data used to validate the parsimonious bimodal $\theta(\psi)$ and K(θ)

The model is validated with data collected across the Canterbury region of New Zealand (Pollacco et al., 2020). The dataset has a sample size of $n = 259$ collected from soil profiles at 46 different sites. Sampled sites include irrigated and non-irrigated pastoral farming land. Rainfall across the sites varies from 550 to 800 mm per year. Soil parent material is sediments derived from quartzo-feldspathic hard sandstone, deposited as either river alluvium or windblown loess (Schmidt et al., 2005). All soils in this study have at least 60 cm depth of fine earth soil material, with most sites classifying to the Pallic soil order in the New Zealand Soil Classification (Hewitt, 2010), correlating in the Soil Taxonomy to Haplusteps and Humustepts great groups. Fourteen sites have younger soils that classify to the recent soil order (Hewitt, 2010), correlating to Haplusteps and Ustifluvent great groups.

Soil was sampled using undisturbed soil cores of 59 cm^3 (5 cm diameter by 3 cm depth) used for $\theta(\psi)$ measurements, and undisturbed soil cores of 589 cm^3 (10 cm diameter by 7.5 cm depth) used for $K(\theta)$ measurements. To ensure consistent θ conditions at all sites, water was infiltrated two days prior to sampling. $\theta(\psi)$ values were measured at 40, 70, 100, 500, 1000, 2000, 4000, 10,000 and 150,000 mm. Measurements less than 1000 mm water pressure head were made on high-flow ceramic plates, with water pressure head applied by a hanging water column, while measurements above 1000 mm water pressure head were made using pressure chambers (Gradwell and Birrell, 1979). To measure $K(\psi)$, the core samples were trimmed, saturated, and equilibrated to 10, 40, 70 and 100 mm water pressure head with a Buchner funnel apparatus, before unsaturated hydraulic conductivity was measured using disc permeameters set to the equivalent water pressure heads for each measurement. Additional detail about the experimental sites, soil sampling and soil physical measurements is given in Pollacco et al. (2020).

3.2. Objective function and goodness of fit

The fitting process that estimates the parameters used an adaptive differential evolution algorithm (Qin et al., 2009; Zhang and Sanderson, 2009) in the BlackBoxOptim.jl library (version 0.5.0, https://github.com/robertfeldt/BlackBoxOptim.jl), written in the Julia language. This procedure used an objective function and goodness-of-fit defined below.

The minimization process between the observed and the fitted values used a weighted objective function, *WOF*, which includes information

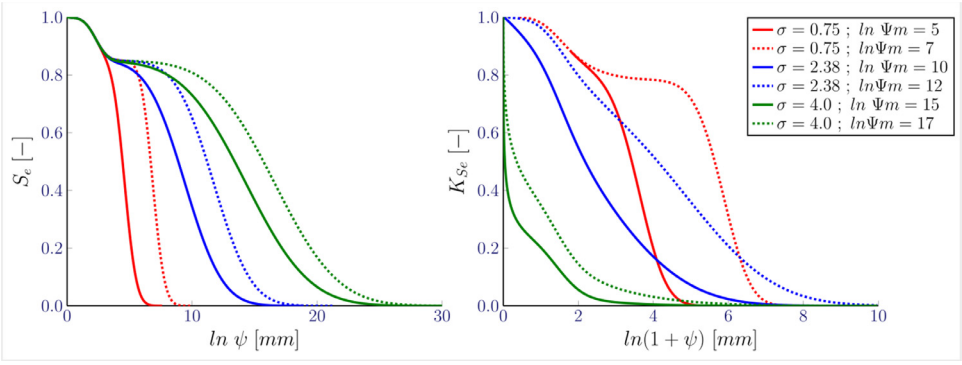

Fig. 3. Example of normalized bimodal hydraulic functions, $S_e(\psi)$ and $K_{Se}(\psi)$, for three different values of σ (0.75, 2.38, and 4.00) and the corresponding feasible range of ψ_m (solid and dotted lines represent hydraulic functions with lower and upper limit respectively) derived from Eq. (12) with $S_e(\theta_{sMac}) = 0.85$.

from both $\theta(\psi)$ and $K(\theta)$ data. The *WOF* is computed as follows:

$$WOF = w\frac{\sum_{i=1}^{l}\left[\theta(\psi)_{obs_i} - \theta(\psi)_{sim_i}\right]^2}{\sum_{i=1}^{l}\left[\theta(\psi)_{obs_i} - \overline{\theta(\psi)_{obs_i}}\right]^2} + (1-w)\frac{\sum_{i=1}^{k}\left[\ln\left(1+K(\theta)_{obs_i}\right) - \ln\left(1+K(\theta)_{sim_i}\right)\right]^2}{\sum_{i=1}^{k}\left[\ln\left(1+K(\theta)_{obs_i}\right) - \overline{\ln\left(1+K(\theta)_{obs_i}\right)}\right]^2} \quad (13)$$

where l and k refer to the total number of experimentally measured data for the $\theta(\psi)$ and $K(\theta)$ curves, respectively (in this case, $l = 9$ and $k = 4$). $\theta(\psi)_{obs_i}$ and $K(\theta)_{obs_i}$ correspond to the observed data derived from the laboratory, and $\theta(\psi)_{sim_i}$ and $K(\theta)_{sim_i}$ correspond to simulated values of the Kosugi model. The weighting parameter, w, rules the relative weight assigned to the fit of the $\theta(\psi)$ and $K(\theta)$, with w set to 0.5 providing the best compromise between the fit of $\theta(\psi)$ and $K(\theta)$ simultaneously.

The goodness of fit of the measured volumetric water retention data to the simulated $\theta(\psi)$ using the bimodal Kosugi model was assessed using the Nash–Sutcliffe efficiency coefficient, $NSE_{\theta(\psi)}$, and the root mean squared error, $RMSE_{\theta(\psi)}$, as follows:

$$NSE_{\theta(\psi)} = \max\left\{1 - \frac{\sum_{i=1}^{l}\left[\theta(\psi)_{obs_i} - \theta(\psi)_{sim_i}\right]^2}{\sum_{i=1}^{l}\left[\theta(\psi)_{obs_i} - \overline{\theta(\psi)_{obs_i}}\right]^2}; 0\right\} \quad (14)$$

$$RMSE_{\theta(\psi)} = \sqrt{\frac{\sum_{i=1}^{l}\left[\theta(\psi)_{obs_i} - \theta(\psi)_{sim_i}\right]^2}{l}} \quad (15)$$

The goodness of fit of the measured hydraulic conductivity data to the simulated $K(\theta)$ using the bimodal Kosugi model was assessed using the Nash–Sutcliffe log efficiency coefficient, $NSLE_{K(\theta)}$, and the root mean squared log error, $RMSLE_{K(\theta)}$, as follows:

$$NSLE_{K(\theta)} = \max\left\{1 - \frac{\sum_{i=1}^{k}\left[\ln\left(1+K(\theta)_{obs_i}\right) - \ln\left(1+K(\theta)_{sim_i}\right)\right]^2}{\sum_{i=1}^{k}\left[\ln\left(1+K(\theta)_{obs_i}\right) - \overline{\ln\left(1+K(\theta)_{obs_i}\right)}\right]^2}; 0\right\} \quad (16)$$

$$RMSLE_{K(\theta)} = \sqrt{\frac{\sum_{i=1}^{k}\left[\ln\left(1+K(\theta)_{obs_i}\right) - \ln\left(1+K(\theta)_{sim_i}\right)\right]^2}{k}} \quad (17)$$

The combined Nash–Sutcliffe efficiency coefficient, $\overline{NSE}$, and root mean squared error, $\overline{RMSE}$, are computed as the average of the previous coefficients for $\theta(\psi)$ and $K(\theta)$:

$$\overline{NSE} = \frac{NSE_{\theta(\psi)} + NSLE_{K(\theta)}}{2} \quad (18)$$

$$\overline{RMSE} = \frac{RMSE_{\theta(\psi)} + RMSLE_{K(\theta)}}{2} \quad (19)$$

3.3. Scenarios in constraining bimodal soil Kosugi hydraulic parameters

Different scenarios (Tables 2 and 3 presented in the results section) to derive the bimodal soil Kosugi hydraulic parameters from inverse modelling are considered using the set of constraints described in Section 2.2. The scenarios are compared to the reference scenario (scenario A) where all hydraulic parameters are optimized except for θ_s which is derived from total porosity. Scenario B derives θ_r from σ, removing one degree of freedom in the optimization scheme; scenarios C and D use a fixed value for σ_{Mac} or ψ_{mMac}, removing two degrees of freedom; scenario E fixes simultaneously σ_{Mac} and ψ_{mMac}, removing three degrees of freedom. Finally, scenarios F and G additionally include dynamically constraining σ and ψ_m, where θ_r is freely optimised or θ_r is derived from σ, respectively.

The relevance of the constraints presented in Section 2.2 to derive the bimodal Kosugi hydraulic parameters is demonstrated by optimizing the parameters exclusively from $\theta(\psi)$ data. In order to compare to the corresponding $K(\theta)$ curve, a known value of K_s is provided from scenario G. Like in the previous approach, degrees of freedom are progressively removed by fixing σ_{Mac} and ψ_{mMac} (scenario H), additionally deriving θ_r from σ (scenario I), and dynamically constraining σ and ψ_m, with θ_r freely optimised and θ_r derived from σ (scenarios J and K respectively).

4. Results

4.1. Parsimonious Kosugi bimodal $\theta(\psi)$ and K(θ) model

This section shows the goodness of fit for $\theta(\psi)$ and $K(\theta)$ for different scenarios where the hydraulic parameters are progressively constrained. The sensitivity for each of the constraints is evidenced by the corresponding decrease in the goodness of fit.

The soil hydraulic parameters (θ_r, σ, ψ_m, K_s, $\theta_{sMacMat}$, σ_{Mac}, and ψ_{mMac}) are optimized using the bimodal $\theta(\psi)$ and $K(\theta)$ model described in Section 2.1. This is performed by matching the simulated $\theta(\psi)$ and $K(\theta)$ values with the experimentally measured data described in Section 3.1. θ_s was not optimized but directly derived from total porosity using measured values of the dry bulk density and particle density (θ_s equals 96.5% of total porosity).

Table 2 summarises the *NSE* coefficients and *RMSE* of the fit between observed and simulated $\theta(\psi)$ and $K(\theta)$ using the different constraints for the hydraulic parameters, as described in Section 2.2. Simulated values for $\theta(\psi)$ and $K(\theta)$ are obtained with the optimized hydraulic parameters in each case (scenario A to G in Table 2). *NSE* values close to 1 as well as *RMSE* values close to 0 indicate perfect agreement between observed and simulated $\theta(\psi)$ and $K(\theta)$.

Table 2 shows that the fit of the bimodal Kosugi hydraulic functions when optimizing the seven hydraulic parameters (scenario A) for the

Table 3
Nash–Sutcliffe log efficiency coefficient ($NSLE_{K(\theta)}$) values and root mean squared log errors ($RMSLE_{K(\theta)}$) from fitting bimodal Kosugi $K(\theta)$ with different constraints of the hydraulic parameters according to Section 2.2 and using the soils described in Pollacco et al. (2020). θ_s is derived from total porosity, σ and $\theta_{sMacMat}$ are optimized for all simulations, and K_s is derived from scenario G in Table 2. N_{opt} is the number of optimized parameters in each case.

Scenario	N_{opt}	θ_r	ψ_m	σ_{Mac}	ψ_{mMac}	$NSLE_{K(\theta)}$	$RMSLE_{K(\theta)}$
H	4	Opt	Opt	$\sigma_{Mac}(\psi_{MacMat})$	$\psi_{mMac}(\psi_{MacMat})$	0.113	0.0044
I	3	$\theta_r(\sigma)$	Opt	$\sigma_{Mac}(\psi_{MacMat})$	$\psi_{mMac}(\psi_{MacMat})$	0.310	0.0031
J	4	Opt	Opt: $\psi_m(\sigma)$	$\sigma_{Mac}(\psi_{MacMat})$	$\psi_{mMac}(\psi_{MacMat})$	0.661	0.0018
K	3	$\theta_r(\sigma)$	Opt: $\psi_m(\sigma)$	$\sigma_{Mac}(\psi_{MacMat})$	$\psi_{mMac}(\psi_{MacMat})$	0.709	0.0017

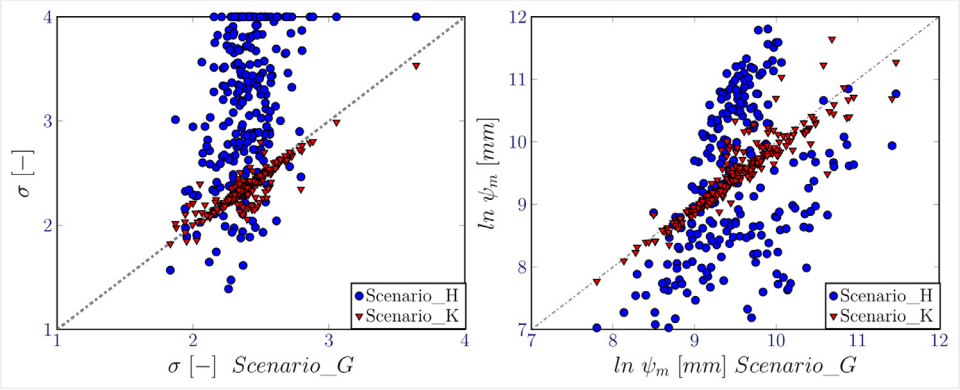

Fig. 4. Comparison between estimated values of σ and ψ_m using scenario H and K (Table 3) with estimated values of σ and ψ_m from scenario G (Table 2). Straight line corresponds to the 1:1 line.

entire data set used in Pollacco et al. (2020) is excellent, with a combined *NSE* very close to unity ($\overline{NSE}$= 0.987) and a combined *RMSE* very close to zero ($\overline{RMSE}$=0.0040). It is expected that reducing the number of optimized hydraulic parameters and constraining them would reduce the goodness of fit. First, the number of optimized parameters was reduced to six (scenario B), deriving θ_r from σ using Eq. (5) as presented in Section 2.2.1, with a marginal decrease in the goodness of fit compared to the scenario A ($\Delta\overline{NSE}$= 0.007 and $\Delta\overline{RMSE}$ = 0.0016). In the next step (scenario C), only five parameters were optimized, by also setting σ_{Mac} as a function of ψ_{MacMat} through Eq. (8) with fixed values for ψ_{MacMat} and P_σ, as described in Section 2.2.2. The goodness of fit is slightly reduced compared to scenario A ($\Delta\overline{NSE}$= 0.015 and $\Delta\overline{RMSE}$ = 0.0018). Next (scenario D), ψ_{mMac} was set as a function of ψ_{MacMat} through Eq. (6) with a fixed value for ψ_{MacMat}, while σ_{Mac} is optimized. This required optimizing five parameters, leading to a small further decrease in the goodness of fit compared to scenario A ($\Delta\overline{NSE}$= 0.023 and $\Delta\overline{RMSE}$ = 0.0020). As expected, σ_{Mac} is more sensitive than ψ_{mMac} to the fit. The combination of the previous two scenarios reduces the number of optimized parameters to four when, apart from relating θ_r to σ, simultaneously setting both σ_{Mac} and ψ_{mMac} as a function of ψ_{MacMat} (scenario E). The reduction in the goodness of fit compared to scenario A is still negligible ($\Delta\overline{NSE}$= 0.027 and $\Delta\overline{RMSE}$ = 0.0023).

To further constrain optimization of the hydraulic parameters, the range of feasible values for σ and ψ_m is dynamically constrained using Eq. (12), as described in Section 2.2.3, so that the combination of both parameters is physically possible. Scenario F, with five optimized parameters, presents the results corresponding to the scenario where σ and ψ_m are dynamically constrained, with σ_{Mac} and ψ_{mMac} set a function of ψ_{MacMat}, and optimizing θ_r freely within its feasible range, as indicated in Table 1. Once again, the reduction of the goodness of fit compared to scenario A remains negligible ($\Delta\overline{NSE}$= 0.063 and $\Delta\overline{RMSE}$ = 0.0033). Finally, scenario G also includes deriving θ_r from σ, reducing to four the number of optimized parameters, with satisfactory goodness of fit compared to scenario A ($\Delta\overline{NSE}$= 0.079 and $\Delta\overline{RMSE}$ = 0.0036). Therefore, scenario G allows a reduction of the number of optimized parameters for the bimodal Kosugi hydraulic model from seven to four without compromising the goodness of fit and while maintaining the hydraulic parameters within their physical limits. Although it is well known that the impact of θ_r in the goodness of fit is significant, this result also highlights the robustness of the constraint associated with this parameter.

4.2. Deriving a unique set of bimodal Kosugi hydraulic parameters from $\theta(\psi)$ data and K_s

To demonstrate the robustness of the proposed methodology, this section shows the relevance of the constraints presented in section 2.2 to derive the bimodal Kosugi hydraulic parameters exclusively from $\theta(\psi)$ data. The full set of hydraulic parameters also requires K_s in order to describe the $K(\theta)$ curve, but this value can be independently obtained either by estimating from $\theta(\psi)$ (Pollacco et al., 2017, 2013b) or measured from infiltration tests (Fernández-Gálvez et al., 2019). Constraining the hydraulic parameters significantly improves the fit of the $K(\theta)$, without using $K(\theta)$ data, and at the same time the estimated hydraulic parameters are physically feasible.

Soil hydraulic data sets do not systematically have experimental measurements of both $\theta(\psi)$ and $K(\theta)$ available to fit the full set of hydraulic parameters (Pollacco et al., 2017). The number of experimentally measured data is larger and with less uncertainty for $\theta(\psi)$ than for $K(\theta)$. This is because $K(\theta)$ is technically more challenging to measure and has higher variability. For the following scenarios the set of experimental data used in this work did not measure K_s. Therefore, the estimated value from scenario G in Table 2 was used as the reference value to derive, using the constraints presented in Section 2.2, the rest of the hydraulic parameters of the bimodal Kosugi functions when only $\theta(\psi)$ data and K_s are available. As shown in Section 4.1, computing σ_{Mac} and ψ_{mMac} from ψ_{MacMat} enables the optimized hydraulic parameters to be more physical and only slightly reduces the goodness of fit. Therefore, in this section we compute σ_{Mac} and ψ_{mMac} from ψ_{MacMat}.

The results presented in Table 3 are organized similarly to Table 2, using different sets of the constraints described in Section 2.2 for the optimization of the hydraulic parameters. Scenario H optimizes four hydraulic parameters, with σ_{Mac} and ψ_{mMac} set as a function of ψ_{MacMat}, and optimizing θ_r freely within its feasible range. In scenario I the number of optimized hydraulic parameters is reduced to three by using the

relationship between θ_r and σ (Eq. (5)), resulting in a small improvement in the goodness of fit for $K(\theta)$. Scenario J required optimizing four hydraulic parameters by dynamically constraining σ and ψ_m through Eq. (12) and using an optimized value for θ_r, resulting in a significant improvement in the goodness of fit. Finally, scenario K optimized three hydraulic parameters, similar to scenario J, but including the constraint of θ_r with σ, resulting in further improvement in the fit for $K(\theta)$. As expected, the $NSLE_{K(\theta)}$ and $RMSLE_{K(\theta)}$ are not as good as in Table 2 because the fit of the hydraulic parameters does not include $K(\theta)$ data. On the other hand, using the constraints presented in Section 2.2 systematically improved the goodness of fit for the hydraulic parameters while keeping them within their physical range.

Fig. 4 compares the optimized σ and ψ_m hydraulic parameters estimated from $\theta(\psi)$ and K_s data using the constraint scenarios H and K, with the values estimated from $\theta(\psi)$ and $K(\theta)$ data using scenario G, which was considered as the reference. The goodness of fit progressively improves from scenario H to K, while the dispersion in the comparison between predicted values to scenario G for σ and ψ_m decreases significantly. Coefficients of determination between predicted values from scenario K and scenario G for σ and ψ_m are 0.999 and 0.934, respectively. Predicted values from scenario K slightly overestimate values obtained from scenario G for σ (slope =0.982) and ψ_m (slope = 0.768).

5. Conclusions

We present in this paper a procedure to derive physical and unique soil hydraulic parameters to describe the bimodal Kosugi hydraulic functions, $\theta(\psi)$ and $K(\theta)$, from inverse modelling. The full methodology is only applicable to the Kosugi hydraulic model, where the representation of the $\theta(\psi)$ and $K(\theta)$ functions is directly related to the pore size distribution. In the proposed approach, θ_s is derived from total porosity, θ_r is derived from σ, ψ_{MacMat} is considered constant, and σ_{Mac} and ψ_{mMac} are derived from ψ_{MacMat}. We also use a dynamic physical constraint in the relationship between σ and ψ_m to reduce non-uniqueness. The constraint for θ_r improves the goodness of fit, although the values used in the expression relating θ_r with σ rely on the fit of experimental data from a specific New Zealand dataset, and it would require validation with data collected from other regions. We describe how to satisfactorily reduce the number of derived hydraulic parameters from eight to four, while ensuring that the derived parameters are physically consistent. Therefore, only σ, ψ_m, $\theta_{sMacMat}$ and K_s are optimized while σ and ψ_m are dynamically constrained. The methodology is easily implemented in an inverse modelling scheme, and the physical constraints also speed up the optimization process.

The goodness of fit between the measured and simulated values from the estimated hydraulic parameters of $\theta(\psi)$ and $K(\theta)$ shows the relevance of the constraints proposed. By progressively constraining the hydraulic parameters, we demonstrate the benefit of the optimal combination of constraints without compromising the fit of the $\theta(\psi)$ and $K(\theta)$ functions. Also, the robustness of the methodology is demonstrated by deriving the bimodal Kosugi hydraulic parameters exclusively from $\theta(\psi)$ and K_s data, enabling satisfactory prediction of $K(\theta)$ without having measured $K(\theta)$ data.

The advantage of deriving optimal hydraulic parameters that are physically sound has a wide range of applications, such as the possibility for better predicting the impact of soil management practices on the pore size distribution (Drewry et al., 2019). Moreover, having a reduced number of hydraulic parameters that are physical reduces uncertainty and allows an improved and faster optimization for characterization of soil hydraulic properties for hydrological and climate modelling. The benefits of using the constraints presented in this paper can also be applied when the hydraulic parameters are inverted from time series of soil water content, the results for which will be presented in a following paper. Additional analyses of constraining the Kosugi hydraulic parameters will also be performed for K_s with methods derived by Pollacco, et al. (2013b) and Pollacco *et al.* (2017). Another benefit of the proposed methodology is that we expect to derive a unique set of hydraulic parameters when the parameters are derived from particle size distribution or infiltration tests (e.g. Pollacco et al., 2020).

Author Statement

Jesús Fernández-Gálvez: Conceptualization, Methodology, Software, Formal analysis, Writing - Original Draft; **Joseph Pollacco:** Conceptualization, Methodology, Software, Formal analysis, Writing - Original Draft; **Linda Lilburne:** Resources, Writing - Review & Editing, Funding acquisition; **Stephen McNeill:** Formal analysis, Writing - Review & Editing; **Sam Carrick:** Resources, Writing - Review & Editing, Funding acquisition; **Laurent Lassabatere:** Validation, Writing - Review & Editing; **Rafael Angulo-Jaramillo:** Validation, Writing - Review & Editing.

Software availability

The software can be downloaded from https://github.com/manaakiwhenua/SoilWater_ToolBox/ and is open source under the GP-3.0 License. This software is part of a set of interlinked modules implemented into the SoilWater-ToolBox ecosystem led by J.A.P Pollacco from Manaaki Whenua – Landcare Research in New-Zealand and J. Fernández-Gálvez from the University of Granada in Spain. The objectives of the SoilWater-ToolBox are to derive the soil hydraulic parameters by using a wide range of cost-effective methods. To date, the following modules are currently included into the SoilWater-ToolBox:

- Intergranular Mixing Particle size distribution model: derives unimodal hydraulic parameters by using particle size distribution (Pollacco et al., 2020);
- General Beerkan Estimation of Soil Transfer parameters method: derives the unimodal hydraulic parameters from single ring infiltration experiments (Fernández-Gálvez et al., 2019);
- Sorptivity model: novel computation of sorptivity used in the General Beerkan Estimation of Soil Transfer parameters method (Lassabatere et al., 2021);
- Derive saturated hydraulic conductivity from unimodal and bimodal $\theta(\psi)$ (Pollacco et al., 2017, 2013b);
- Invert hydraulic parameters from θ time series (Pollacco et al., 2021);
- Derive unique and physical bimodal Kosugi hydraulic parameters as in this paper.

Declaration of Competing Interest

The authors declare that they have no known competing financial interests or personal relationships that could have appeared to influence the work reported in this paper.

Acknowledgements

This research was funded by the Ministry of Business, Innovation and Employment's Endeavour Fund, through the Manaaki Whenua-led 'Next Generation S-map' research programme, C09 × 1612. We would like to thank from Manaaki Whenua – Landcare Research John Dando for the laboratory physical determinations, Veronica Penny for collecting soil cores and samples, and John Drewry for reviewing the manuscript. Mathieu Sellier from Civil Mechanical of the University of Canterbury (New Zealand) is also thanks for reviewing the manuscript.

References

Beven, K., 1993. Prophecy, reality and uncertainty in distributed hydrological modelling. Adv. Water Resour. Res. Perspect. Hydrol. 16, 41–51. https://doi.org/10.1016/0309-1708(93)90028-E.

Brooks, R.H., Corey, A.T., 1964. In: Hydraulic properties of porous media, 27. Colorado State University, Fort Collins, p. 3 Hydrology Papers 3.

Carrick, S., Almond, P., Buchan, G., Smith, N., 2010. In situ characterization of hydraulic conductivities of individual soil profile layers during infiltration over long time periods. Eur. J. Soil Sci. 61, 1056–1069. https://doi.org/10.1111/j.1365-2389.2010.01271.x.

Clapp, R.B., Hornberger, G.M., 1978. Empirical equations for some soil hydraulic properties. Water Resour. Res. 14, 601–604. https://doi.org/10.1029/WR014i004p00601.

Drewry, J.J., McNeill, S.J., Carrick, S., Lynn, I.H., Eger, A., Payne, J., Rogers, G., Thomas, S.M., 2019. Temporal trends in soil physical properties under cropping with intensive till and no-till management. N.Z. J. Agric. Res. 1–22. https://doi.org/10.1080/00288233.2019.1684323.

Du, C., 2020. Comparison of the performance of 22 models describing soil water retention curves from saturation to oven dryness. Vadose Zone J. 19, e20072 10/gjk3p5.

Durner, W., 1994. Hydraulic conductivity estimation for soils with heterogeneous pore structure. Water Resour. Res. 30, 211–223. https://doi.org/10.1029/93wr02676.

Fernández-Gálvez, J., Pollacco, J.A.P., Lassabatere, L., Angulo-Jaramillo, R., Carrick, S., 2019. A general Beerkan Estimation of Soil Transfer parameters method predicting hydraulic parameters of any unimodal water retention and hydraulic conductivity curves: Application to the Kosugi soil hydraulic model without using particle size distribution data. Adv. Water Res. 129, 118–130. https://doi.org/10.1016/j.advwatres.2019.05.005.

Gradwell, M.W., Birrell, K.S., 1979. Methods for physical analysis of soils. New Zealand Soil Bureau scientific report 10C. Department of Scientific and Industrial Research, New Zealand. https://doi.org/10.7931/DL1-SBSR-10C.

Hewitt, A.E., 2010. New Zealand Soil Classification. Landcare Research Science Series No.1, 3rd edition Manaaki Whenua Press, Lincoln, New Zealand.

Ines, A.V.M., Droogers, P., 2002. Inverse modelling in estimating soil hydraulic functions: a Genetic Algorithm approach. Hydrol. Earth Syst. Sci. Discuss. 6, 49–66 10/fwc66m.

Ines, A.V.M., Mohanty, B.P., 2008. Near-surface soil moisture assimilation for quantifying effective soil hydraulic properties using genetic algorithm: 1. Conceptual modeling. Water Resour. Res. 44 10/dwk4jt.

Jarvis, N.J., 2007. A review of non-equilibrium water flow and solute transport in soil macropores: principles, controlling factors and consequences for water quality. Eur. J. Soil Sci. 58, 523–546. https://doi.org/10.1111/j.1365-2389.2007.00915.x.

Kosugi, K., 1996. Lognormal Distribution Model for Unsaturated Soil Hydraulic Properties. Water Resour. Res. 32, 2697–2703. https://doi.org/10.1029/96WR01776.

Kosugi, K., 1994. Three-parameter lognormal distribution model for soil water retention. Water Resour. Res. 30, 891–901.

Lassabatere, L., Di Prima, S., Bouarafa, S., Iovino, M., Bagarello, V., Angulo-Jaramillo, R., 2019. BEST-2K Method for Characterizing Dual-Permeability Unsaturated Soils with Ponded and Tension Infiltrometers. Vadose Zone J. 18, 1–20. https://doi.org/10.2136/vzj2018.06.0124.

Lassabatere, L., Yilmaz, D., Peyrard, X., Peyneau, P.E., Lenoir, T., Šimůnek, J., Angulo-Jaramillo, R., 2014. New analytical model for cumulative infiltration into dual-permeability soils. Vadose Zone J. 13. https://doi.org/10.2136/vzj2013.10.0181, 0.

Lassabatere, L., Peyneau, P.-E., Yilmaz, D., Pollacco, J., Fernández-Gálvez, J., Latorre, B., Moret-Fernández, D., Di Prima, S., Rahmati, M., Stewart, R.D., Abou Najm, M., Hammecker, C., Angulo-Jaramillo, R., 2021. Scaling procedure for straightforward computation of sorptivity. Hydrol. Earth Syst. Sci. Discuss. https://doi.org/10.5194/hess-2021-150, 0.

Lee, T.-K., Ro, H.-M., 2014. Estimating soil water retention function from its particle-size distribution. Geosci. J. 18, 219–230. https://doi.org/10.1007/s12303-014-0017-7.

Leij, F.J., Alves, W.J., Van Genuchten, M.T., Williams, J.R., 1999. The UNSODA unsaturated soil hydraulic database. In: Proceedings of the International Workshop on Characterization and Measurement of the Hydraulic Properties of Unsaturated Porous Media, pp. 1269–1281.

Luxmoore, R.J., 1981. Micro-, meso-, and macroporosity of soil. Soil Sci. Soc. Am. J. 45, 671–672 10/dsfn9p.

McLeod, M., Aislabie, J., Ryburn, J., McGill, A., 2008. Regionalizing potential for microbial bypass flow through New Zealand soils. J. Environ. Qual. 37, 1959–1967. https://doi.org/10.2134/jeq2007.0572.

Mohammadi, M.H., Meskini-Vishkaee, F., 2013. Predicting soil moisture characteristic curves from continuous particle-size distribution data. Pedosphere 23, 70–80.

Pollacco, J.A.P., Angulo-Jaramillo, R., 2009. A Linking Test that investigates the feasibility of inverse modelling: application to a simple rainfall interception model for Mt. Gambier, southeast South Australia. Hydrol. Processes 23, 2023–2032. https://doi.org/10.1002/hyp.7329.

Pollacco, J.A.P., Braud, I., Angulo-Jaramillo, R., Saugier, B., 2008a. A Linking Test that establishes if groundwater recharge can be determined by optimising vegetation parameters against soil moisture. Ann. Forest Sci. 65. https://doi.org/10.1051/forest:2008046.

Pollacco, J.A.P., Ugalde, J.M.S., Angulo-Jaramillo, R., Braud, I., Saugier, B., 2008b. A linking test to reduce the number of hydraulic parameters necessary to simulate groundwater recharge in unsaturated soils. Adv. Water Resour. 31, 355–369. https://doi.org/10.1016/j.advwatres.2007.09.002.

Pollacco, J.A.P., Fernández-Gálvez, J., Carrick, S., 2020. Improved prediction of water retention curves for fine texture soils using an intergranular mixing particle size distribution model. J. Hydrol. 584, 124597. https://doi.org/10.1016/j.jhydrol.2020.124597.

Pollacco, J.A.P., Mohanty, B.P., 2012. Uncertainties of water fluxes in soil-vegetation-atmosphere transfer models: inverting surface soil moisture and evapotranspiration retrieved from remote sensing. Vadose Zone J. 11. https://doi.org/10.2136/vzj2011.0167.

Pollacco, J.A.P., Binayak, B.P., Efstratiadis, A., 2013a. Weighted objective function selector algorithm for parameter estimation of SVAT models with remote sensing data. Water Resour. Res. 49, 6959–6978. https://doi.org/10.1002/wrcr.20554.

Pollacco, J.A.P., Nasta, P., Ugalde, J.M.S., Angulo-Jaramillo, R., Lassabatere, L., Mohanty, B.P., Romano, N., 2013b. Reduction of feasible parameter space of the inverted soil hydraulic parameters sets for Kosugi model. Soil Sci. 178 (6), 267–280. https://doi.org/10.1097/SS.0b013e3182a2da21.

Pollacco, J.A.P., Webb, T., McNeill, S., Hu, W., Carrick, S., Hewitt, A., Lilburne, L., 2017. Saturated hydraulic conductivity model computed from bimodal water retention curves for a range of New Zealand soils. Hydrol. Earth Syst. Sci. 21, 2725–2737. https://doi.org/10.5194/hess-21-2725-2017.

Pollacco, J.A.P., Fernández-Gálvez, J., Carrick, S., McNeill, S., Peltzer, D.A., Belfort, B., Ackerer, P., Lassabatere, L., Angulo-Jaramillo, Zammit, S.C., Rajanayaka, C., 2021. HyPix: 1D Richards equation hydrological model in Julia language using multistep optimization scaling for flexible vertical soil discretization.. Submitted to Environmental Modelling & Software Manuscript Number: ENVSOFT-D-21-00501.

Qin, A.K., Huang, V.L., Suganthan, P.N., 2009. Differential evolution algorithm with strategy adaptation for global numerical optimization. IEEE Trans. Evol. Computat. 13, 398–417 10/bz6hs5.

Romano, N., Nasta, P., 2016. How effective is bimodal soil hydraulic characterization? Functional evaluations for predictions of soil water balance. Eur. J. Soil Sci. 67, 523–535. https://doi.org/10.1111/ejss.12354.

Schmidt, J., Almond, P.C., Basher, L., Carrick, S., Hewitt, A.E., Lynn, I.H., Webb, T.H., 2005. Modelling loess landscapes for the South Island, New Zealand, based on expert knowledge. N.Z. J. Geol. Geophys. 48, 117–133. https://doi.org/10.1080/00288306.2005.9515103.

Sonkar, I., Kotnoor, H.P., Sen, S., 2019. Estimation of root water uptake and soil hydraulic parameters from root zone soil moisture and deep percolation. Agric. Water Manage. 222, 38–47 10/ghsgfr.

Timlin, D.J., Ahuja, L.R., Ankeny, M.D., 1994. Comparison of three field methods to characterize apparent macropore conductivity. Soil Sci. Soc. Am. J. 58, 278–284 10/fqs29h.

van Genuchten, M.T., 1980. A closed-form equation for predicting the hydraulic conductivity of unsaturated soils. Soil Sci. Soc. Am. J. 44, 892–898.

Wösten, J.H.M., Lilly, A., Nemes, A., Le Bas, C., 1999. Development and use of a database of hydraulic properties of European soils. Geoderma 90, 169–185. https://doi.org/10.1016/S0016-7061(98)00132-3.

Zhang, Sanderson, A.C., 2009. JADE: adaptive differential evolution with optional external archive. IEEE Trans. Evol. Computat. 13, 945–958 10/d883z7.